Nanoscale

Dynamic self-assembly of detonation nanodiamond in water

Journal:	*Nanoscale*
Manuscript ID	NR-COM-10-2019-008984.R1
Article Type:	Communication
Date Submitted by the Author:	07-Feb-2020
Complete List of Authors:	Chang, Shery; Arizona State University, LeRoy Eyring Center for Solid State Science Reineck, Philipp; RMIT University, ARC Centre of Excellence for Nanoscale BioPhotonics & School of Science Williams, Dewight; Arizona State University Bryant, Gary; RMIT University, School of Science; RMIT University, Centre for Molecular and Nanoscale Physics Opletal, George; CSIRO, Molecular & Materials Modelling Data61 Eldemrmash, Samir; RMIT University, School of Science Chiu, Po-Lin; Arizona State University, School of Molecular Sciences Osawa, Eiji; NanoCarbon Research Institute, Barnard, Amanda; CSIRO, Data61 Dwyer, Christian; Monash University, Monash Cente for Electron Microscopy

Journal Name

ARTICLE TYPE

Cite this: DOI: 10.1039/xxxxxxxxxx

Dynamic self-assembly of detonation nanodiamond in water†

Shery L. Y. Chang,*[a,b] Philipp Reineck,[c] Dewight Williams,[a] Gary Bryant,[d] George Opletal,[e] Samir A. El-Demrdash,[d] Po-Lin Chiu,[b] Eiji Ōsawa,[f] Amanda S. Barnard,[e] and Christian Dwyer[g]

Received Date
Accepted Date

DOI: 10.1039/xxxxxxxxxx

www.rsc.org/journalname

Nanodiamonds are increasingly used in many areas of science and technology, yet, their colloidal properties remain poorly understood. Direct imaging as well as light and x-ray scattering reveal that purified detonation nanodiamond (DND) particles in an aqueous environment exhibit a self-assembled lace-like network, even without additional surface modification. Such behaviour is previously unknown and contradicts the current consensus that DND exists as mono-dispersed single particles. With the aid of mesoscale simulations, we show that the lace network is likely the result of competition between a short-ranged electrostatic attraction between faceted particles and a longer-ranged repulsion arising from the interaction between the surface functional groups and the surrounding water molecules which prevents complete flocculation. Our findings have significant implications for applications of DND where control of the aggregation behaviour is critical to performance.

Applications of detonation nanodiamond (DND) include lubricants[1,2], mechanical strengthening agents for nanocomposites[3,4], and seed materials for diamond film growth[5,6], as well as more-recent biomedical applications including drug delivery[7–14], biosensing[15–17] and biolabelling[18–20]. Detonation synthesis[21,22] yields diamond nanoparticles 3–5 nm in size which typically exhibit diamond cores and fullerene-like shells[23,24], giving them unique surface properties which are extremely useful in a wide range of applications[25,26]. The performance of DND in many applications is critically dependent on the dispersion behaviour in solution. For example, in drug delivery (e.g., of the widely-used chemotherapy drug doxorubicin hydrochloride[7,9], or the common antibiotic tetracycline[27]) an efficient loading of drug molecules relies on mono-dispersed particles to maximize the available surface area[27]; on the other hand, the often-desireable slow release of the drug requires the formation of nanodiamond aggregates[7]. Such examples highlight the crucial importance of understanding and thereby controlling the DND dispersion behaviour.

DND synthesis is notorious for producing large tightly-bound agglutinates composed of diamond nanoparticles, graphitic phases and amorphous-carbon phases[28]. Hence considerable effort has been spent developing methods to break down and purify the agglutinates into mono-dispersed primary particles. These methods use bead-milling, often followed by chemical and/or thermal treatment to further remove undesired graphitic surface layers[28–30]. The resulting purified DND is generally believed to be monodispersed with narrow size distribution and high colloidal stability[5,26,28,31]). We emphasize that the DND purification methods do not involve the use of surfactants for dispersion, and so they are rather different from the methods often used in

[a] Eyring Materials Center, Arizona State University, Tempe, USA. E-mail: shery.chang@asu.edu
[b] School of Molecular Science, Arizona State University, Tempe, USA.
[c] ARC Centre of Excellence for Nanoscale BioPhotonics, School of Science, RMIT University, Melbourne, Australia.
[d] School of Science, RMIT University, Melbourne, Australia.
[e] Data61, CSIRO, Docklands, Australia.
[f] NanoCarbon Research Institute, Ueda, Japan.
[g] Department of Physics, Arizona State University, Tempe, USA.

† Electronic Supplementary Information (ESI) available: (1) Detailed description of the DND synthesis; (2) Details of DLS and SAXS experiments; (3) cryo-TEM specimen preparation and imaging; (4) atomic and electronic structures of DND; (5) mesoscale simulations of nanodiamond aggregation; and (6) Effect of surface chemistry from the purification process to the DND aggregates.

‡ Acknowledgment: SLYC, DW , PC, CD and MAR acknowledge the use of TEMs and FT-IR at Eyring Materials Center at Arizona State University. P.R. acknowledges funding through the RMIT Vice-ChancellorÕs Research Fellowship. PR, GB and SAE acknowledge the Australian Microscopy and Microanalysis Research Facility at RMIT University. Computational resources for this project were supplied by the National Computational Infrastructure national facility under Partner Allocation Scheme, Grant q27.

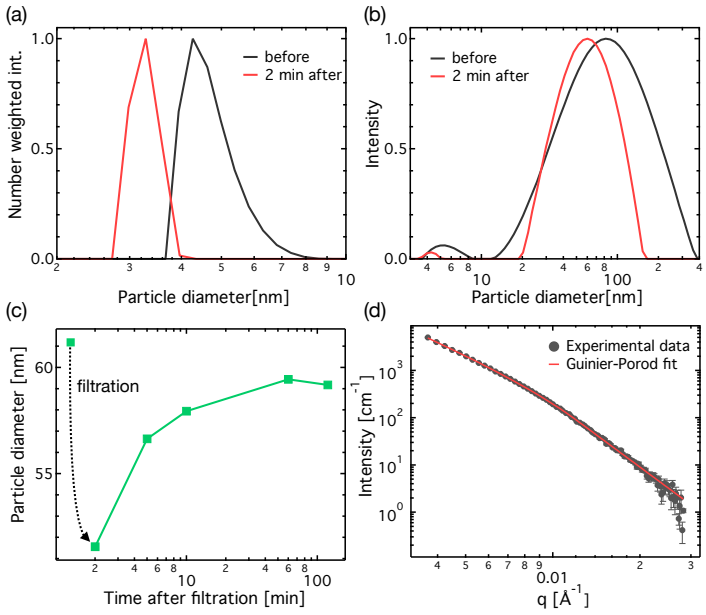

Fig. 1 DLS and SAXS measurements of DND particles dispersed in water (1 mg mL^{-1}). (a) number weighted particle size distribution before (black line) and after (red lines) filtration; (b) intensity-weighted distribution before and after filtration; (c) time evolution of mean particle diameter determined by cumulant analysis; and (d) SAXS intensity (data points) and Guinier-Porod fit (red line).

metal, metal oxide, and semiconductor colloidal systems, where surfactants in the form of polymers, organic molecules or proteins promote and stabilize the particle dispersions[32]. However, contradicting observations of DND dispersion have been reported recently, thereby calling into question the current consensus. For example, recent water absorption measurements suggest that DND in water consists of random aggregates with meso- and micropores[33]. In addition, unexpectedly high viscosities have been reported, which far exceed theoretical estimates based on the assumption of mono-dispersion[31,34].

Here, we report definitive measurements of the dispersion behaviour of DND in aqueous environments using direct imaging in a transmission electron microscope under cryogenic conditions (cryo-TEM), together with the complementary dynamic light scattering (DLS) and small angle x-ray scattering (SAXS). We show that, in the absence of surface modification or surfactants, DND particles exhibit a remarkable self-assembly to form lace-like networks. Such networks are composed primarily of ordered chain- and rope-like aggregates which are formed by connecting facets of individual DND particles. Using first-principles calculations and additional experiments described below, we propose that the lace network results from an electrostatic attraction between faceted nanoparticles and a repulsion arising from the interaction between the surface functional groups and water molecules in the aqueous medium, which stabilizes such chain-like aggregates against further random aggregation.

Firstly we examine the particle size distribution of the as-received DND dispersed in water (1 mg mL^{-1}) and the potential existence of aggregates based on our DLS measurements (ALV-5022F light scattering spectrometer with a laser wavelength of 633 nm). Fig. 1(a) (black line) shows the commonly-used number weighted particle size distribution obtained for the as-received material. This plot shows a single peak at 4.5 nm, suggesting that DND is monodispersed in water with a primary particle size of 4.5 nm, in agreement with the existing literature and the consensus view. However, this representation can be slightly misleading as it assumes that the particles are monodispersed and spherical, and by converting to a number distribution it conceals the presence of larger particles such as aggregates. Fig. 1(b) (black line) shows the raw intensity-weighted distribution, which is more sensitive to larger particles/aggregates since the scattered intensity is proportional to the particle diameter to the sixth power. This plot clearly shows two broad peaks, one at 5 nm and another at around 80 nm, the latter indicative of larger aggregates (although their relative concentration can only be determined on the assumption of spherical particles). Thus the sample contains isolated particles (highlighted in Fig. 1(a)) and aggregates (highlighted in Fig. 1(b), which dominate the scattering). The third representation (Fig. 1(c)) provides an intensity weighted *average* particle size which requires no *a priori* assumptions but does not provide the distribution of sizes. This representation allows us to observe temporal trends more easily.

In order to determine if the large aggregates are the by-product of the purification process (*i.e.* the DND suspension being a mixture of stable single primary particle and stable aggregates), or if the aggregation is a dynamic process, DLS measurements were also performed as a function of time after the DND dispersion was filtered using a syringe filter with a pore size of 220 nm (Fig. 1(a)–(c)). Fig. 1(c) shows that filtration results in a reduction of the average particle/aggregate size from 61 nm to 50 nm. However the average size begins to increase immediately after filtration, reaching an equilibrium value of 60 nm after one hour. If the aggregates were static (*e.g.* a by-product of the purification process), there would be no growth following filtration. These results thus demonstrate that the aggregation is dynamic in nature, a situation which we refer to as a dynamic equilibrium.

The shape of aggregates was analyzed using SAXS. Fig. 1(d) shows the scattered x-ray intensity as a function of scattering vector (data points). The Guinier-Porod fit (red line) yields a dimensionality parameter of 0.3 (for which values of 3, 2 and 1 correspond to spheres, rods and plates, respectively), suggesting that the aggregates have an elongated structure. Taken together, the DLS and SAXS results suggest that aggregates in the form of elongated structures exist in the DND dispersion, and that they exist in a dynamic equilibrium.

Light and x-ray scattering experiments are indirect measurements that provide valuable information about particle ensembles. In order to directly and unambiguously determine the aggregate morphology of the DND in water, we utilised cryo-TEM imaging, which enables direct imaging of the native state of a DND dispersion in an aqueous solution via vitrification. The DND dispersion sample with the concentration of 1 w/v % was frozen using a plunge-freezing method[35] (which is commonly used to 'fix' biological materials containing large fractions of water). The process of rapid cooling transforms (within microseconds) water into vitreous ice, thereby preserving the native state of the

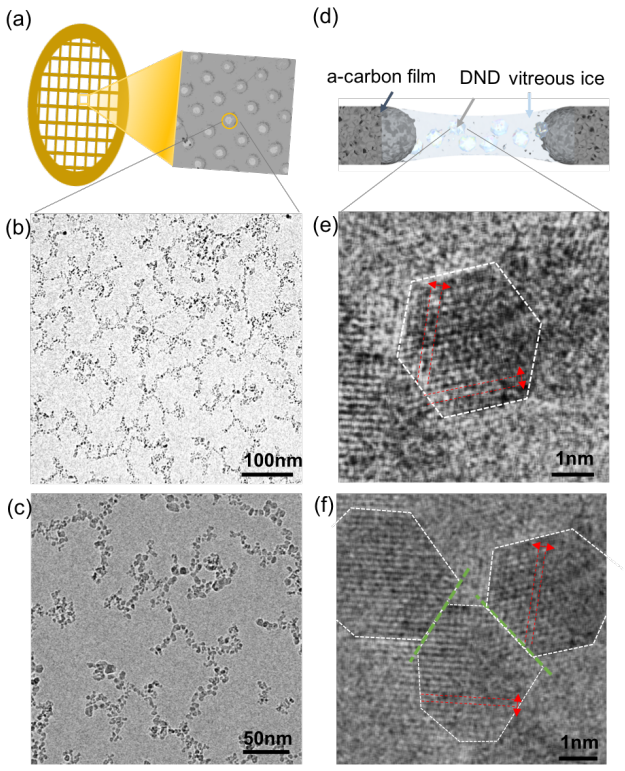

Fig. 2 Cryo-TEM images of unmodified nanodiamond in water. (a) and (d) Schematic diagram of a vitrified specimen for cryo-TEM; (b) typical area of a cryo-TEM image of nanodiamond in water; (c) enlarged image from (b); (e) high magnification cryo-TEM image of an single polyhedron nanodiamond particle truncated by {111} surfaces. Red dotted lines indicate {111} lattice planes; and (f) interfaces (highlighted with the green dotted lines) of three nanodiamond particles in a chain.

DND aggregates in solution (a schematic diagram is shown in Fig. 2(a)). Fig. 2(b) shows that the DND in vitreous ice has a striking lace-like network. The enlarged image in Fig. 2(c) reveals that such networks are composed of chain- and rope-like aggregates, and no individually dispersed DND was observed. This is in stark contrast to the current understanding of DND dispersion. At high magnification, the diamond lattice of the DND particles is clearly revealed and the particles appear as polyhedrons which are seen in projection (Fig. 2(d-e)). We note that it is extremely rare to see such high-resolution lattice information (1.9 Å for diamond (111)) using cryo-TEM imaging due to the stringent limits on the radiation dose for imaging materials in vitreous ice. Here such information allows us to characterise the facets and interfaces of nanodiamond particles in an aqueous environment.

Close examination of the lace-like network shows that it contains three types aggregate morphologies, which we refer to as 'chains,' 'ropes,' and 'random clusters.' The chain morphology, an example of which is shown in Fig. 3(a), is an ordered aggregate formed by connecting facets of individual DND particles (another example of a chain appears in Fig. 2(f)). Chains in our definition here have a nominal width of one particle. An example of the rope morphology is shown in Fig. 3(b). Ropes are similar to chains but they are composed of up to three nanodiamond particles in width. Moreover, ropes can develop multiple branches,

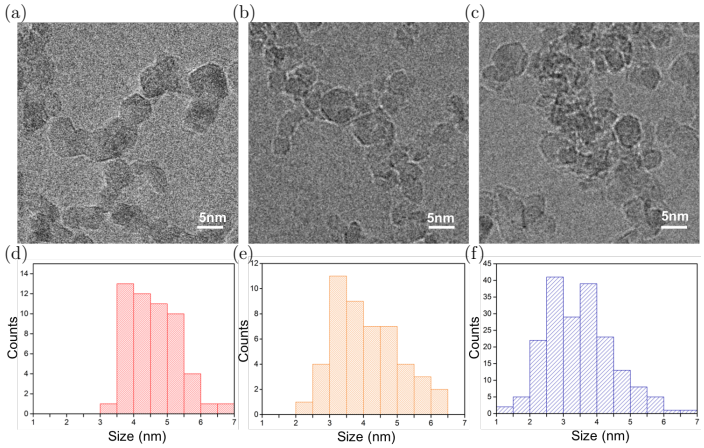

Fig. 3 Cryo-TEM images of aggregate morphologies and their corresponding particle size distributions. (a) chain, (b) rope, (c) random cluster, (d)-(f) the particle-size distributions corresponding to the chain, rope and cluster morphologies, respectively.

where each branch tends to have the chain structure. The third morphology, which comprises a smaller fraction among the three morphologies, is the random cluster, shown in Fig. 3(c). The particle interconnections within the random clusters do not appear to have any systematic attributes. Further analysis reveals that the different morphologies contain different particle-size distributions: particles that form chains have a relatively narrow size distribution, whereas the particles that form ropes and clusters have increasingly larger size distributions, as shown in Fig. 3(d)–(f).

The cryo-TEM results provide conclusive evidence that the the DND dispersion consists mostly of chain- and rope-like aggregates. This is in excellent agreement with our DLS and SAXS findings that the presence of large aggregates in the suspension have elongated structures. It should be noted that the assembly of nanoparticles through connecting facets of individual particles is very unusual as colloidal particle assembly typically involves surfactants, which prevent direct contact of particle facets. In order to understand why the lace-network is the stable structure, we have considered the following three factors: the role of specific functional groups on the DND surfaces, the particle-particle electrostatic interactions between pristine nanodiamond surfaces, and the interaction of the surface functional groups with the water surrounding the DND particles.

DND particle surfaces are known to contain multiple coexisting functional groups including ketones, aldehydes, amines, hydroxyl and hydrogen, which are leftover from the purification process[25,26]. We have analyzed two DND suspensions with similar primary particle size but with different surface chemistries resulting from different purification processes, one rich in carboxylic groups (sample provided by Adámas Nanotechnologies) and the other rich in C-H groups (sample provided by NanoCarbon Research Institute. see SI for details for both materials). Since these two types of surface groups have *opposite* charges, it is expected that the dispersion behaviour should differ if surface chemistry has a dominating effect. However, the lace network persists in

both suspensions with extremely similar morphologies (see Fig. S4). This result strongly suggests that the specific surface functional groups alone are not responsible for creating and stabilising the lace network. Moreover, the fact that the lace-network persist for DNDs with both positively and negatively charged surface groups confirms that such assembly is independent of the purification process.

Next we consider the electrostatic interactions between faceted nanodiamond particles. Density functional theory based calculations have predicted that pristine nanodiamond polyhedra can exhibit non-uniform surface charges while maintaining overall charge neutrality[36]. Particles with oppositely-charged surfaces can attract to form chains and loops[36,37]. To examine if such interactions can give rise to the lace-network, we conducted first-principles-parametrized simulations of the mesostructures generated by 25,000 faceted polyhedral nanodiamond particles, with varying sizes and shapes containing {100}, {110} and {111} facets. Neither surface groups nor water are included in the simulations (see SI for details). In the representative view of the simulation cell in Fig. 4(a) it can be seen that the simulations did not predict the lace-network as observed in the cryo-TEM experiments. The simulation nonetheless show chains, ropes and clusters, as well as a very small fraction of individual particles. However, whereas our experimental observations show that a significant proportion of the aggregates are chains and long ropes, the simulations predict that clusters are the dominant morphology. To represent the simulation results, we have plotted in Fig. 4(b) the average particle coordination as a function of the aggregate size. (The average particle coordination is the particle coordination normalized by the number of the particles in the aggregate. A long chain has an average coordination of 2, whereas a cluster has a higher average coordination.) In Fig. 4(b) we see the trend that small aggregates tend to be chains/ropes and larger aggregates are clusters, and that varying the concentration does not change this trend.

Our mesoscale simulations described above provide strong evidence that electrostatic attractions between faceted particles give rise to chain/rope aggregates in the DND suspensions. To form a chain, the faceted particles must be well-matched to each other, which is reflected in our experimentally observed narrower (and $>$3 nm) particle-size distribution in Fig. 3(d). On the other hand, the interaction between the functional groups present on DND surface and the surrounding water molecules has recently been shown to induce hydrogen-bond network of water molecules in aqueous dispersion[38]. This hydrogen-bond network has been acknowledged for the good colloidal stability of DND[38]. We therefore proposed that electrostatic attractions between faceted particles produce chain/rope aggregates, and that these aggregates are stabilized against further flocculation by the repulsion force arising from the hydrogen-bond network surrounding the aggregates. In our mesostructure simulations there is no such repulsion preventing chains/ropes from continuing to interact electrostatically, which explains why clusters become the dominant aggregate morphology in our simulations.

In conclusion, DND particles exhibit unusual self-assembly forming lace-like network in water which is not previously known. The lacey network is composed predominantly of chain and rope aggregate morphologies, and some fraction of clusters. Such behaviour contradicts the current belief that purified DND in water exists as mono-dispersed single particles. We have demonstrated that the lacey network can be robust with respect to the specific purification processes required by the synthesis. We have shown that the formation of such a lacey network is likely due to the combined effect of electrostatic interactions between faceted particles, which promote the formation of chains/ropes, and longer-ranged repulsions arising from the interaction between the surface functional groups and the surrounding water, which stabilize the chains/ropes against further aggregation. Such findings have a profound impact on the use of DND where the applications rely on the control of aggregation (particle-particle interaction) and DND interaction with the surrounding species including solvent, substrate and other bio-molecules. In the case of recently-developed drug delivery applications, our findings reveal that the large surface area available due to the lacey network is extremely beneficial for the uptake of the drug molecules. Further control of the aggregate behaviour of purified DND is possible to achieve by taking advantage of the size-dependent aggregate morphologies, by modifying the surfaces of DND, or by manipulating the solution medium. Selecting particles with a narrower size distribution can increase the fraction of chains and ropes that give maximum surface area, whereas a broader size distribution can increase the fraction of clusters where nano-sized pores within the clusters can be utilised. Alternatively, manipulation of the solution medium can be used to tune the aggregation between chains/ropes and clusters. Such possibilities offer attractive routes for optimizing DND for its designated applications.

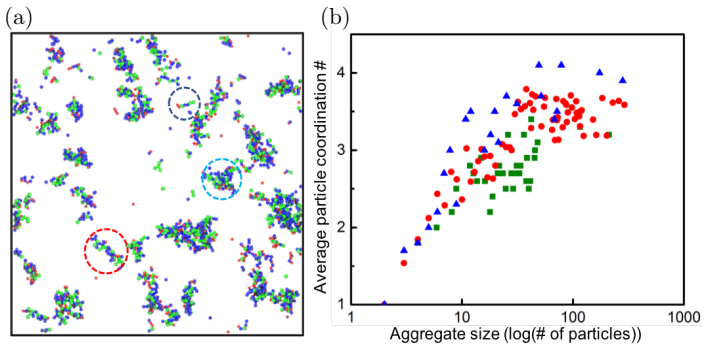

Fig. 4 Simulations of nanodiamond assembly calculated using 25,000 particles of three different shapes and size range 2.2–3.2 nm in a 242.5^3 nm^3 cell. (a) representative view of aggregates at a concentration of 1.75×10^{18} particles/cm^3 with 2.2, 2.7 and 3.2 nm particles shown in red, blue and green, respectively. The black dotted circle highlights the chain morphology, the red dotted circle the rope morphology and the blue dotted circle the cluster morphology; (b) the average particle coordination number as a function of the aggregate size for three particle concentrations of 4.38×10^{17} (green), 1.75×10^{18} (red), and 3.5×10^{18} (blue) particles/cm^3.

References

1 O. Ivanov, M.; Shenderova, *Curr. Opin. Solid State Mater. Sci.*, 2016, **21**, 17.
2 C. C. Chou and S. H. Lee, *Wear*, 2010, **269**, 757.

3 V. Livramento, J. B. Correia, N. Shohoji and E. Osawa, *Diamond Relat. Mater.*, 2007, **6**, 202.
4 I. Neitzel, V. Mochalin, I. Knoke, G. R. Palmese and Y. Gogotsi, *Compos. Sci. Technol.*, 2011, **71**, 710.
5 O. A. Williams, O. Douheret, M. Daenen, K. Haenen, E. Osawa and M. Takahashi, *Chem. Phys. Lett.*, 2007, **445**, 255.
6 O. Shenderova, S. Hens and G. McGuire, *Diamond Relat. Mater.*, 2010, **19**, 260.
7 E. K. Chow, X. Zhang, M. Chen, R. Lam, E. Robinson, H. Huang, D. Schaffer, E. Ōsawa, A. Goga and H. Dean, *Sci. Trans. Med.*, 2011, **3**, 73ra21.
8 A. Schroeder, D. Heller, M. Winslow, J. Dahlman, G. Pratt, R. Langer, T. Jacks and D. Anderson, *Nat. Rev.*, 2012, **39**, 12.
9 S. Mitragotri, D. G. Anderson, X. Chen, E. K. Chow, D. Ho, A. V. Kabanov, J. M. Karp, K. Kataoka, C. A. Mirkin, S. H. Petrosko, J. Shi, M. M. Stevens, S. Sun, S. Teoh, S. S. Venkatraman, Y. Younan Xia, S. Wang, Z. Gu and C. Chenjie Xu, *ACS Nano*, 2015, **9**, 6644.
10 D. Ho, C. K. Wang and E. K. Chow, *Sci. Adv.*, 2015, **1**, e1500439.
11 U. Roy, V. Drozd, A. Durygin, J. Rodriguez, P. Barber, X. Atluri, V. abnd Liu, T. G. Voss, S. Saxena and M. Nair, *Scientific Report*, 2018, **8**, 1603.
12 Z. Cui, Y. Zhang, K. Xia, Q. Yan, H. Kong, J. Zhang, J. Zuo, X. Zuo, J. Shi, L. Wangg, Y. Zhu and C. Fan, *Nature Communications*, 2018, **9**, 4347.
13 S. Wei, L. Li, X. Du and Y. Li, *J. Mater. Chem. B*, 2019, **7**, 3390.
14 D. Bhowmik, G. K. Dhindsa, U. R. Shrestha, E. Mamontov and X.-q. Chu, *arXiv e-prints*, 2016, arXiv:1609.02656.
15 W. Zhang, K. Patel, A. Schexnider, S. Banu and A. D. Radadia, *ACS Nano*, 2014, **8**, 1419.
16 Z. Wang and Z. Dai, *Nanoscale*, 2015, **7**, 6420.
17 S. Claveau, J.-R. Bertrand and F. Treussart, *Micromachines*, 2018, **9**, 247.
18 G. Hong, S. Diao, A. L. Antaris and H. Dai, *Chem. Rev.*, 2015, **115**, 10816.
19 L. M. Manus, D. J. Mastarone, E. A. Waters, X. Zhang, E. A. Schultz-Sikma, K. W. MacRenaris, D. Ho and T. J. Meade, *Nano Lett.*, 2010, **10**, 484.
20 N. Nunn, M. dÕAmora, N. Prabhakar, A. M. Panich, N. Froumin, M. D. Torelli, I. Vlasov, P. Reineck, B. Gibson, J. M. Rosenholm, S. Giordani and O. Shenderova, *Methods Appl. Fluoresc.*, 2018, **6**, 035010.
21 E. Ōsawa, *Pure Appl. Chem.*, 2008, **80**, 1365.
22 V. V. Danilenko, *Phys. Solid State*, 2004, **46**, 595.
23 L. Y. Chang, A. S. Barnard, C. Dwyer, C. B. Boothroyd, R. K. Hocking, E. Ōsawa and J. Nicholls, *Nanoscale*, 2016, **8**, 10548.
24 J. Raty, G. Galli, C. Bostedt, T. W. van Buuren and L. J. Terminello, *Phys. Rev. Lett.*, 2003, **90**, 037401.
25 V. N. Mochalin, O. Shenderova, D. Ho and Y. Gogotsi, *Nature Nanotechnology*, 2012, **7**, 11.
26 E. Ōsawa, *Chemistry of Nanocarbons*, John Wiley & Sons, 2010, ch. 17.
27 J. Giammarco, V. N. Mochalin, J. Haeckel and Y. Gogotsi, *J. Colloid Interface Sci.*, 2016, **6**, 261.
28 A. Krueger, F. Kataoka, M. Ozawa, T. Fujino, Y. Suzuki, A. E. Aleksenskii, A. Y. Vul and E. Ōsawa, *Carbon*, 2005, **43**, 1722.
29 B. J. M. Etzold, I. Neitzel, M. Kett, F. Strobl, V. N. Mochalin and Y. Gogotsi, *Chem. Mater.*, 2014, **26**, 3479.
30 O. Shenderova and N. Nunn, *Nanodiamonds*, Elsevier, 2017, ch. 2.
31 A. Y. Vul, E. D. Eidelman, A. E. Aleksenskiy, A. V. Shvidchenko, A. T. Dideikin, V. S. Yuferev, V. T. Lebedev, Y. V. KulÕvelis and M. V. Avdeev, *Carbon*, 2017, **114**, 242.
32 M. Grzelczak, J. Vermant, E. M. Furst and L. M. Liz-Marzán, *ACS Nano*, 2010, **4**, 3591.
33 E.-Z. Pina-Salazar, K. Urita, T. Hayashi, R. Futamura, F. Vallejos-Burgos, J. Wloch, P. Kowalczy, M. Wi?niewski, T. Sakai, I. Moriguchi, A. P. Terzyk, E. Osawa and K. Kaneko, *Langmuir*, 2017, **33**, 11180.
34 N. M. Kuznetsova, S. I. Belousov, D. Y. Stolyarova, A. V. Bakirov, S. N. Chvalun, A. V. Shvidchenkod, E. D. Eidelman and A. Y. Vul, *Diamond & Related Materials*, 2018, **83**, 141.
35 J. Dubochet and A. W. McDowall, *J. Microscopy*, 1981, **124**, 3.
36 A. S. Barnard and E. Ōsawa, *Nanoscale*, 2014, **6**, 1188.
37 L. Y. Chang, E. Ōsawa and A. S. Barnard, *Nanoscale*, 2011, **3**, 958.
38 T. Petit, H. Yuzawa, M. Nagasaka, R. Yamanoi, E. Ōsawa, N. Kosugi, and E. F. Aziz, *J. Phys. Chem. Lett.*, 2015, **6**, 2909.

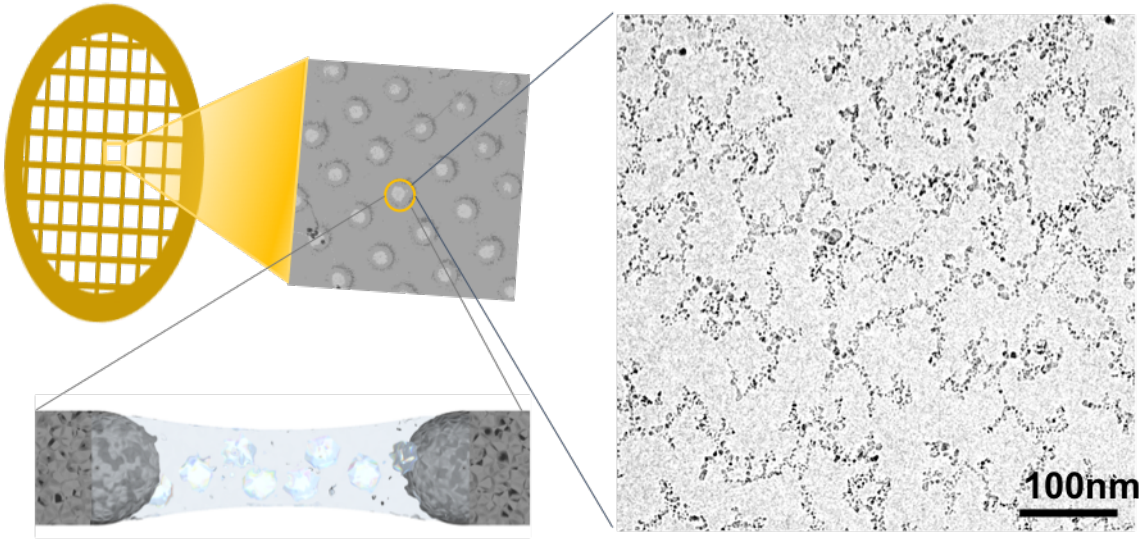

Previously unknown dynamic self-assembly of purified detonation nanodiamond dispersion in water without any additional surface modification.